Solar Energy Materials & Solar Cells 287 (2025) 113246

Contents lists available at ScienceDirect

Solar Energy Materials and Solar Cells

journal homepage: www.elsevier.com/locate/solmat

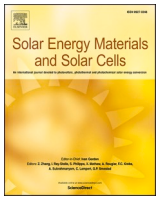

A smart semi-translucent building-integrated PV module based on integrated-tracking micro-concentration providing high power density and active daylight management

Almudena Garcia-Sanchez [a,*], Guido Vallerotto [a], Steve Askins [a], Ignacio Antón [a], César Domínguez [a,b]

[a] Instituto de Energía Solar, Universidad Politécnica de Madrid, Av. Complutense 30, 28040, Madrid, Spain
[b] ETS Ingeniería y Diseño Industrial, Universidad Politécnica de Madrid, Spain

ARTICLE INFO

Keywords:
Solar energy
Concentrator photovoltaics
Building-integrated photovoltaics
Micro-concentrator optics

ABSTRACT

Building-integrated photovoltaics (BIPV) can support the green energy transition by enabling building envelopes as solar generators. However, current development rates are insufficient, partly due to the low efficiency of conventional semi-transparent modules and the difficult integration of the high-glare illumination they produce. This work introduces a smart semi-translucent double-glazed BIPV module utilizing concentrator photovoltaics with integrated tracking. The module concentrates direct irradiance on the solar cells to produce electricity and allows transmission of diffuse irradiance to create comfortable daylighting with very low glare, avoiding the need of blinds. Depending on user needs, tracking can be switched to a high-transmission mode, where direct light is deviated from the cells towards the interior of the building to increase daylighting. This concept can be integrated into roof components (e.g., a skylight), façade components (e.g., a curtain wall) or other exterior elements (e.g., solar shading) of buildings. The optical design employs asymmetric linear Fresnel lenses to concentrate light on an array of 2.3 mm-wide solar cells strips (10X). The focal line moves with solar position, so the cell plane is shifted to collect concentrated light using a micro-tracking system. We evaluate optical efficiency, angular tolerance, and daylighting properties using ray-tracing simulations with realistic material and solar properties. A peak efficiency of 76 % is obtained and it is kept above 60 % for transverse angles of incidence beyond 55° when a secondary optical element is added. Furthermore, photorealistic rendering demonstrates the comfortable daylighting (low glare) produced by the module, showcasing its advantages over conventional semi-transparent BIPV.

1. Introduction

The cumulative photovoltaic (PV) capacity in Europe would need to reach 455–605 GW to meet the ambitious European Green Deal target of a 55 % net reduction in greenhouse gas emissions by 2030, and being climate-neutral by 2050 [1]. This will require an efficient use of the available land of our cities, for instance through building-applied photovoltaics (BAPV) and building-integrated photovoltaics (BIPV). However, at current growth rates, BAPV and BIPV installations in Europe will only reach 5 GW in 2030 [2]. A faster market penetration may be promoted via technology breakthroughs able to raise module efficiency and adding smart functions like the active daylighting management [3].

BIPV increases the amount of envelope surface of the building useable for PV and brings additional functions [4]. These modules replace conventional parts of the building so they must follow the strict mechanical, electrical, and fire safety requirements as any construction element and additionally help to increase thermal and acoustic insulation. The combination of PV cells and structural glazing results in transparent, semitransparent, and translucent PV modules that can be integrated on the façade or the roof of a building to generate electricity and produce daylighting. Typical commercial semitransparent BIPV modules use a double glazing in which opaque c-Si solar cells are laminated leaving a space between them to allow some light to pass through and illuminate the interior of the building. However, this spacing reduces electrical efficiency dramatically compared to BAPV modules, so they show a low power density (peak power per unit area).

* Corresponding author.
E-mail address: almudena.garcia@upm.es (A. Garcia-Sanchez).

https://doi.org/10.1016/j.solmat.2024.113246
Received 30 June 2024; Received in revised form 29 September 2024; Accepted 20 October 2024
Available online 2 April 2025

Furthermore, system costs for BIPV curtain walls ranging 600–1000 €/m^2 make that them hardly competitive in terms of cost per watt peak due to their low efficiency. Thus, increasing power density is essential to prop up their adoption. Furthermore, semi-transparency of opaque cells produces hard shadows and bright illumination fringes inside the building that can create a high visual discomfort to end users, which further hinders adoption by building designers.

Concentrator photovoltaics (CPV) has since long been proposed by many teams as a way to increase BIPV module efficiency and manage daylighting properties: [5]. CPV uses optical elements to concentrate direct irradiance on small solar cells in order to increase their efficiency and save semiconductor area, which in turns reduces the carbon footprint of the generated electricity [6]. Furthermore, since the large angular spread of diffuse irradiance cannot be concentrated, it can be transmitted through the system to provide low-glare daylighting inside the building. However, increasing geometrical concentration (ratio of optical aperture area to solar cell area) limits the angular acceptance of the system, so moving tracking systems are required to point to the incident sunlight beam unless concentration is low. Thus, most published concepts of building-integrated concentrator photovoltaics (BICPV) systems are static concepts with a very low geometrical concentration, relying typically on metallic reflective or solid dielectric concepts [7–11]. However, these systems become thick and heavy, and the complexity introduced is hardly justified by the small semiconductor savings and yearly energy yield. Besides, mirrors and thick optical paths leave a small transparency for diffuse light to produce useful daylighting. Other concepts specifically designed to regulate daylighting, which can be referred to as BICPV/D, often rely on seasonal adjustments. For instance, Wu et al. [12] proposed a window with passive thermal actuation to switch optical functions: for the winter months with low temperatures, the window is totally clear to increase daylighting and solar thermal load; under the summer high temperatures, an inner thermotropic layer makes most of the incident solar radiation to be back scattered and conducted through the cover glass (acting as light pipe) to the solar cells at the edges of the module. However, optical efficiency is very low due to the scattering and the long optical path. Fresnel lenses are known to achieve a high optical efficiency with minimal thickness and material consumption. Valencia-Caballero et al. [3] demonstrated a BICPV skylight module with seasonal solar behavior based on stripes of static linear Fresnel lenses alternating with strings of solar cells. In summer, the lenses deviate solar radiation at high solar elevation towards the solar cells, thus creating ~2X concentration. In winter, low-elevation sunlight is deviated towards the interior of the building. Overall, the yearly gain in solar electricity is 10 %, but daylighting still produces hard shadows and high glare. In both systems, daylighting is governed by external circumstances that cannot be controlled by the user and the effective concentration is very low.

In order to introduce active daylighting control, static linear Fresnel lenses have been proposed in combination with tracking receivers that capture the concentrated direct sunlight at the focal line as it moves with solar position, while the diffuse fraction is allowed to enter the building to produce illumination without a sharp contrast [13]. In the pioneering [14] and the most recent [15] versions of this idea, concentrated light is captured using domed Fresnel lenses to avoid mutual shading between facets when sunlight is not normal to the lens aperture. However, a curved design cannot be easily integrated into practical BIPV products and can hardly be produced using glass, the standard material for transparent building envelopes. Furthermore, due to the large aperture area of the Fresnel lens considered, a thermal absorber is added to dissipate the large amount of heat entering the solar cell. The resulting hot fluid may provide an added value to building users, but the heat transfer installation dramatically increases installation complexity and can hardly be justified in terms of installation, operation and maintenance costs.

In this work we present a novel smart translucent BICPV/D module based on narrow flat linear Fresnel lenses with integrated tracking capabilities and active daylighting control depending on user needs or ambient conditions. This module is designed to simultaneously generate electricity with high efficiency and homogeneous daylighting with low glare, thus improving the energy balance of the building towards net zero and the comfort of users. Furthermore, the optical concept has been tailored to ultraviolet roll-to-plate imprinting processes, which enable low-cost, high-throughput production of large-area micro-optical arrays on typical building glass glazing. Thus, the system presented can be easily adapted to conventional building envelope systems, such as curtain walls, skylights or canopies. This article describes the structure, operation principles and optical design of the concept. Its performance in terms of optical efficiency, angular tolerance and daylighting properties is assessed using Monte-Carlo ray tracing simulations. This study offers a comprehensive understanding of the module's functionality, showcasing its ability to optimize both energy production and natural lighting within buildings.

2. Structure and working principle of the proposed module concept

A sketch of the proposed module architecture is shown in Fig. 1. The front cover can be a single or double glazing on which the array of primary optical elements (POE) is molded using ultraviolet nanoimprint lithography (UVNIL) [16]. Each POE is a linear Fresnel lens that concentrates direct irradiance onto solar cell strips placed on the backplane, which is moved to accommodate focal line displacements due to varying solar position by means of a planar micro-tracking system. Solar cells may be coupled with secondary optical elements (SOE) to improve the angular tolerance of the system. Moreover, the backsheet is made transparent to allow the transmission of diffuse irradiance into the building as low-glare daylighting. Direct light is blocked by the solar cells and converted into electricity. However, depending on the user needs or ambient conditions, the micro-tracking system can displace solar cells out of the foci and allow transmission of direct light into the building for increased daylighting or solar gain. Thus, the system can be switched between low- and high-transmission modes, or be modulated between these two extremes.

The module is designed to be used as a translucent element of the building envelope. It can be integrated into horizontal roofing elements (e.g., atrium skylights or canopies) and vertical façade elements (e.g., curtain walls) where no direct view of the exterior is required (e.g. upper and lower fractions of the façade of each floor). It functions as a solar shading device, preventing direct irradiance from entering the building,

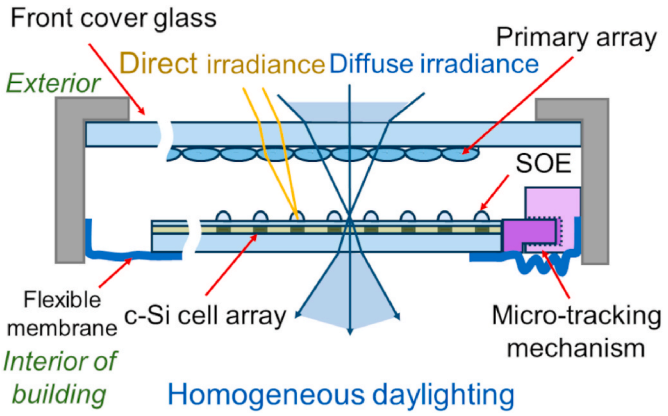

Fig. 1. Sketch of the semi-translucent smart BIPV module concept based on micro-CPV. Direct light is concentrated to produce electricity, while diffuse light is transmitted for daylighting. A micro-tracking mechanism shifts the backplane, so the concentrated light is cast on the cells over a wide range of solar incidence angles.

thereby reducing thermal load.

The primary lens array would be typically fabricated on the innermost face of a flat solar-control glass or an insulated glazing unit (IGU, e.g., a double-glazing structure with inner insulated Argon-filled cavity), so that the variations in thickness of the glazing do not affect the focal distance or optical behavior of the lens. Solar control strategies such as reflective coatings to reduce heat load and ultraviolet rays or low-emissivity coatings to improve heat insulation can be added to the opposite face of the primary lens glass pane (e.g., inner cavity of a double glazing) and will not affect its concentration performance as long as the glazing is kept transparent (coatings must not produce light scattering). These will further enhance the module's performance by meeting typical thermal and acoustic insulation requirements.

3. Optical design methodology

3.1. Concentrator architecture and design rationale

Elements to be integrated in buildings must comply with structural and geometrical constraints regardless their final purpose. In this case, the total thickness of the smart BIPV module must be similar to a conventional curtain wall. Therefore, the initial design constraint imposed was a maximum module frame thickness of 10 cm. Consequently, leaving some overhead thickness of 2.5 cm to accommodate front glass, backplane and mechanical actuators, the design focal length of the linear Fresnel lens was set to 7.5 cm. In order to maximize the concentration ratio of the lens, a conservative f-number f/# > 1.5 was chosen (focal distance divided by lens width) [17] and set to 1.7, which results

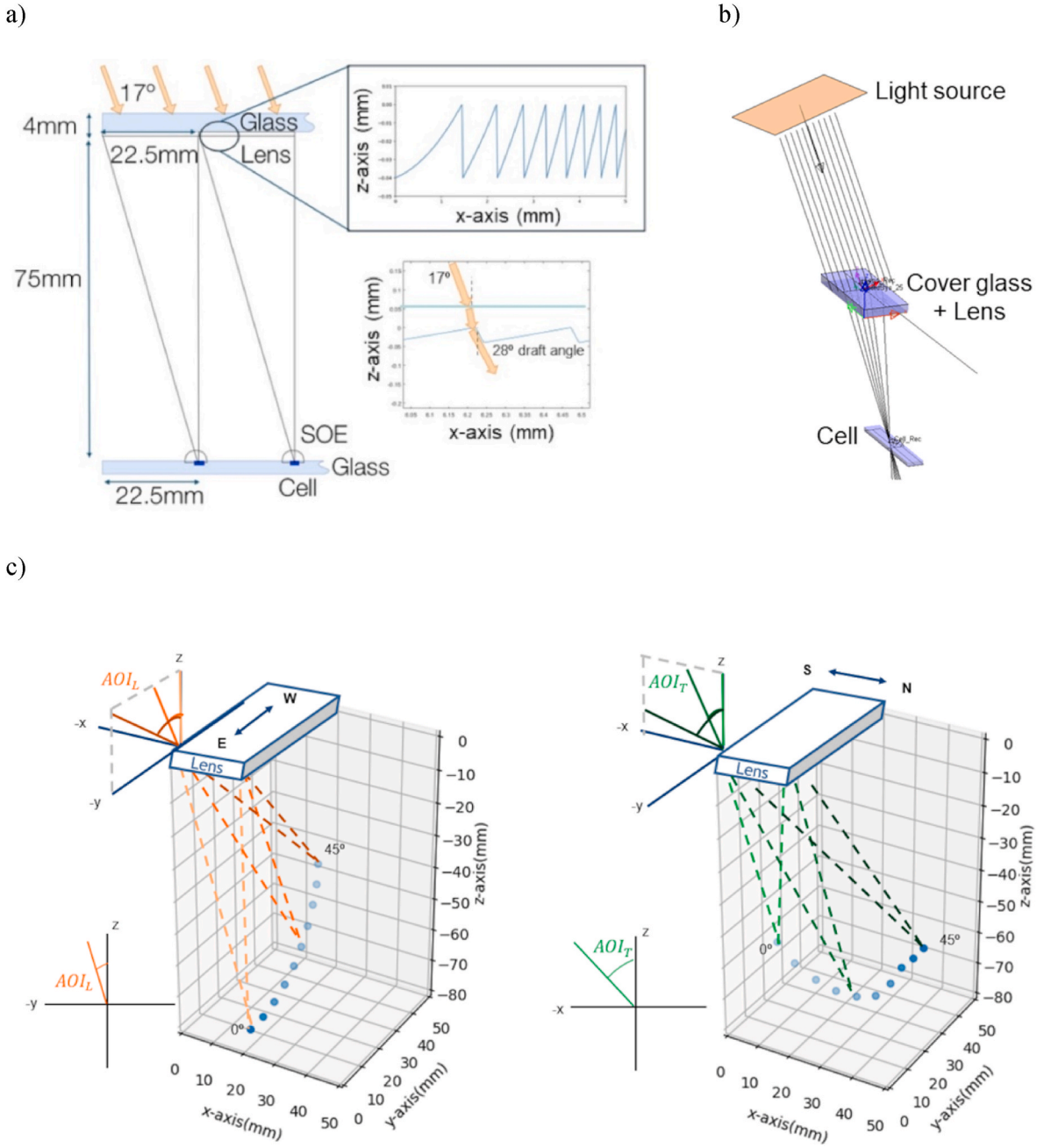

Fig. 2. a) Schematic of the optical design at nominal AOI, together with close-up of the asymmetric Fresnel lens profile. b) Setup modeled using a commercial ray-tracing software. c) Representation of the angle of incidence in the longitudinal plane (AOI_L) of the lenses and the angle of incidence across the cross section of the lenses (AOI_T), and their effect on the focal line position.

in a lens width of 4.5 cm. These type of linear Fresnel lenses are commonly used in CPV [18–20].

Conventional CPV system designs aim to perfectly concentrate the light with normal angle of incidence (AOI = 0°). In contrast, in this case, regardless the specific configuration (roofing or façade), the AOI varies across a wide range of angles throughout the day and the year and it depends on the latitude and orientation of the installation. For instance, in a building in Madrid (the latitude for which the proposed design was optimized), the AOI at noon on a horizontal plane varies between 17° and 63° from summer to winter solstices, respectively. Thus, the optical design must maintain a resonable concentration over a wide range of AOIs. When the axis of symmetry of the linear lens is east-west oriented, AOI at noon is transverse to the lens (AOI_T) and the angle of incidence longitudinal to the lens is zero ($AOI_L = 0$).

Fig. 2 **a)** shows a schematic of the optical architecture at the design AOI. The design of the lens profile (bidimensional) was generated using Fermat's principle, so that light rays with the design angle of incidence reach the same point (focus) at the edge of the lens section. In common linear Fresnel lenses designed for normal light incidence, usually half of the lens is designed and then it is mirrored to obtain a symmetric linear profile. Thus, they work similarly for both positive and negative AOI_T values. In this case, however, the design must work exclusively for positive AOI_T much greater than zero (17°–63°), so the mirrored half would produce large total internal reflection losses. Therefore, the mirrored half is spared, which results in an asymmetric aspheric linear Fresnel lens with a width of 22.5 mm (half of the full width obtained using the f-number definition). The minimum AOI_T (17°) was chosen for the final design to maximize the optical efficiency of the concentrator under the maximum solar heat load conditions (where the solar beam is most perpendicular to the module). When AOI_T varies, it is expected that the focal line moves following a Petzval field curvature. Ray-tracing simulations were used to locate these field curvatures for angles of incidence both tranverse (AOI_T) and longitudinal (AOI_L) to the linear lenses, as shown in Fig. 2 c. Variations in AOI_T produce a displacement in focal distance (z axis) and the direction transverse to the lens (x axis). Variations in AOI_L produce a displacement in the direction longidutinal to the lens (y axis), but also in the z axis again. If the substrate with solar cells is shifted to accommodate these focal changes, ray tracing shows that an optical efficiency higher than 60 % can be maintained for a geometrical concentration of 2.8X in the AOI_T range 17°–63°. Moreover, as it will be seen later in section 4, adding a secondary optical element (SOE) allows to increase the concentration up to 10X maintaining the same angular tolerance.

The draft angle of the Fresnel facets is fixed to 28° to reduce mutual shading at high AOI_T. The facet height is set to 40 μm to enable cost-effective production through roll-to-plate UV micro-imprinting. This manufacturing process achieves not only economical optical quality replication but it is also scalable to a continuous large-area process. In this process, a UV-curable resin is pressed by a roller mold drum onto a flat substrate (solar glass), while a UV lamp cures the resin from behind the substrate. This method reduces production costs and time compared to traditional batch processing of concentrator lenses, making the proposed module more economically feasible than other concentration-based concepts.

3.2. Optical modeling

The performance of the optical system was modeled in a 3D environment using a commercial ray-tracing software based on Monte-Carlo simulations. Fig. 2 b**)** shows an example of the 3D setup under a collimated light beam at the reference AOI. For the light source, we used the AM1.5D direct spectrum, and an angular aperture of ±0.27° to recreate the direct irradiance of the Sun. Cells of two different widths of 2.25 mm and 8 mm have been defined as receivers to explore two different geometrical concentrations: 10X and 2.8X, respectively. Fresnel reflection losses and optical properties of the materials (dispersion and spectral absorption) have been included in the simulation model. The power collected at the receiver has been weighted by the spectral response of a conventional c-Si solar cell to estimate the effect of sunlight in photocurrent and provide an effective optical efficiency. For the daylight analysis study, we recreated a 3D room environment using standard reflection properties for the wall (80 %), and we added a secondary light source to simulate diffuse radiation (a half sphere with isotropic emission). Moreover, angles of incidence are varied in the planes both longitudinal (AOI_L) and transverse to the lenses (AOI_T). We can transform any solar angle to this system from azimuth and elevation by projecting them onto the YZ and XZ planes of the lens system, as shown in Fig. 2c).

3.3. Tracking trajectory

To assess the performance of the designed optical system and to study the trajectory of the planar tracking we simulated the solar trajectory (described by AOI_L and AOI_T) corresponding to the most representative days of the year, *i.e.* summer and winter solstices as limit positions, and the spring and autumn equinoxes as middle positions, for a south-oriented horizontal skylight in Madrid. Fig. 3a), left shows a sketch of the trajectory of the sun on the representative days. Incidence angles AOI_L and AOI_T are derived from the solar position (azimuth and elevation). Then, using ray-tracing simulations we determined the optimum position of the solar cell (i.e. the position which maximizes the light capture) along the transverse (x) and focal (z) axes (see Fig. 2c) for a representation of the system coordinates). As shown in Fig. 2c), the focal lines move in the axis longitudinal to the lenses (y axis), but this displacement of few centimeters is very small compared to the typical width of the module in this dimension (hundreds of cm). Thus, if the strip solar cells in the same row are connected in parallel to act as a single cell with an aggregate width similar to that of the module, not tracking across the y-axis introduces a small loss in the total photocurrent. Furthermore, tracking in this dimension would require the solar cells backplane to move beyond the lens array section, which involves leaving large spare margins at the module edges. This would reduce power density significantly in exchange of a very small energy gain at large AOI_L values (low plane-of-array irradiance) and much higher complexity of the mechanical tracking system. Moreover, as the receiver gets closer to the concentrator along z axis, the required y-axis displacement reduces accordingly. Therefore, no tracking will be implemented in practice for the y axis. Note that the results presented in the next section incorporate this limitation.

The resulting tracking trajectories in the z- and x-axis are represented in the graph in Fig. 3a), right. Therefore, to ensure that the planar tracking can follow the light foci throughout the year, the backplane should be able to move about 5.5 cm on the z-axis and 4.5 cm on the x-axis, a relatively small displacement in comparison with the dimensions of a commercial module ($1 \times 2\ m^2$).

3.4. Secondary optical element design to increase light collection

As the sun position deviates from the design angle of incidence over the lenses, the focus width increases, resulting in a lower optical efficiency caused by the light spilled out of the receiver (see later in section 4.1). To maximize the direct light capture throughout the year there are two options: reducing the system concentration or including a SOE in the system. Both options have been simulated and compared. Again, an iterative process has been carried out to identify the optimum design angle. However, in this case the best results have been obtained dividing the SOE in two sections and designing each one of them for a different design angle. In particular, the right and left part of the dome redirect the light beam to the center of the solar cell when the AOI_T of the light is 17° and 63°, respectively. Fig. 3b) shows the resulting asymmetric SOE profile.

In the next section the optical efficiency of the system as a function of

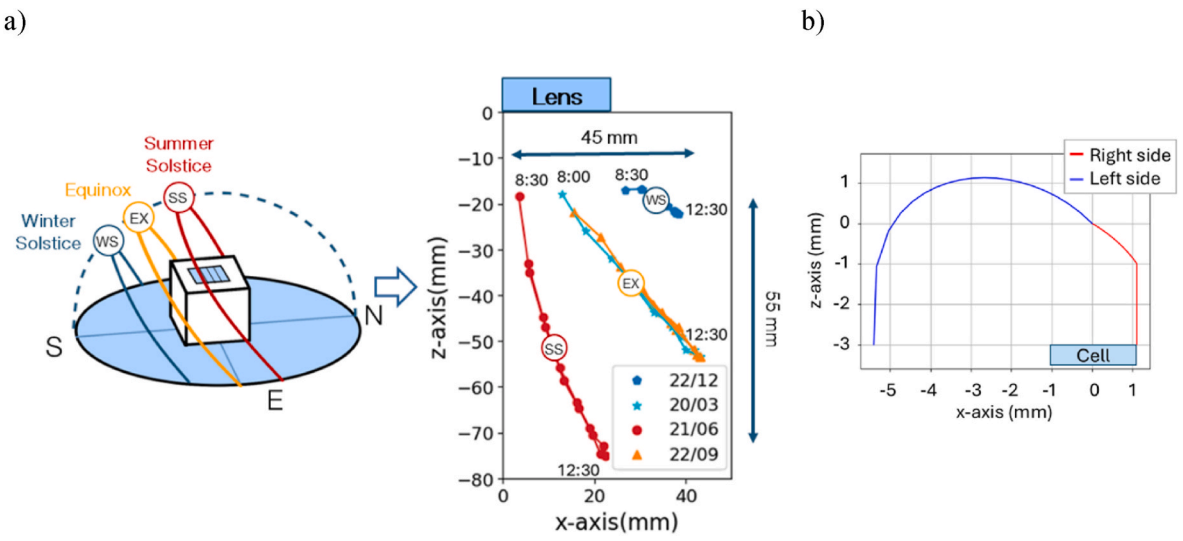

Fig. 3. a) Graphic representation of the solar path and the two-stage x-z linear tracking movement for the most representative days of the year: the summer (red line) and winter (dark blue line) solstice as limit positions and spring (soft blue line) and autumn (orange line) equinox as middle positions. b) asymmetric refractive dome SOE profile.

the AOI_T will be presented for the 10X without SOE configuration, the 2.8X without SOE configuration, and the 10X with SOE configuration.

4. Results and discussion

4.1. Optical efficiency versus angle of incidence

The optical system was simulated to assess its performance in terms of optical efficiency and angular tolerance. Three different receiver configurations have been considered, all based on lamellar c-Si solar cells: a 2.3-mm width bare cell (10X), an 8-mm width bare cell (2.8X) and a 2.3-mm width cell with the SOE. The simulation traces rays varying the AOI_T between 17° and 63° and, for each simulated angle, the receiver is placed in the position which maximizes the light capture. The results are shown in Fig. 4a. Firstly, the 10X system with a bare 2.3-mm cell achieves an optical efficiency of 76 % at 27°, but drops quickly for AOI_T beyond 30°. Reducing the concentration from 10X to 2.8X leads to significantly increasing the angular tolerance, which keeps optical efficiency higher than 60 % up to 55°. Secondly, adding the SOE to the 10X system improves the angular tolerance in the same amount at the cost of a small reduction in efficiency caused by reflection and absorption in the SOE. However, the peak efficiency loss is highly compensated by the improved angular tolerance, which would increase significantly the energy generated daily. Thus, the 10X configuration with SOE is probably the best trade-off between higher power density and lower semiconductor usage. Note that for all the three configurations, the maximum efficiency does not correspond to the lower AOI_T. The draft angle of the facets has been intentionally designed to minimize shelf-shadowing at this peak angle. This decision aims to achieve a balance between maintaining stable optical efficiency across a wide range of angles and minimizing light loss at AOI_T values close to 0°, for which the solar flux received is maximum.

Finally, in order to estimate the energy performance of buildings equipped with this type of module, it is necessary to model its behavior throughout the year. To this end, the optical efficiency has been modeled as a function of all possible AOI_T and AOI_L values for the 2.8X system (best case) using ray tracing simulations. Fig. 4b shows a color map representing the calculated values, along with the tracking trajectories for the most representative days of the year: summer solstice (SS), equinoxes (EX) and winter solstice (WS), in black lines. Please note that the AOI_L values represent both positive and negative values, which are symmetric, while only positive AOI_T values are useful. For most of the relevant operating conditions optical efficiency is above 70 %, which demonstrates the robustness of the design and a high PV yield.

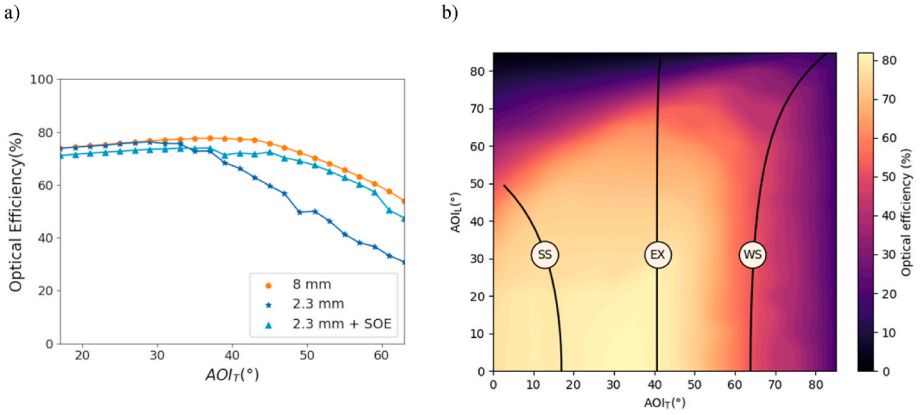

Fig. 4. a) Optical efficiency vs. **AOI_T** for different receivers: 8-mm cell (2.8X), 2.3-mm cell (10X) and 2.3-mm cell with SOE (10X). b) Optical efficiency as a function of the transverse and longitudinal angles of incidence on the 8-mm cell (2.8X) configuration. Black lines indicate tracking trajectories for the most representative days of the year: summer solstice (SS), equinoxes (EX) and winter solstice (WS).

4.2. Daylighting properties

A reference office scene was created to analyze daylighting properties of the BICPV/D module used as a skylight and to benchmark it against other glazing systems. They were evaluated using the same ray-tracing software, which is able to run simulations in photometric units and to perform a photorealistic rendering of the scene under direct and diffuse irradiance. In order to reduce computational needs, a small room at 1:5 scale was modeled with dimensions 0.5 m × 0.7 m x 0.6 m, (equivalent to 2.5 m × 3.5 m x 3 m), including the 2.8X configuration module as a square 0.2 m × 0.2 m skylight (equivalent to 1 m × 1 m). Fig. 5 shows the results of the photorealistic rendering of daylighting for a typical clear-sky spring day at noon in Madrid latitude ($AOI_T = 45°$). The wall on the left faces north. Apart from the smart BICPV/D module, a classic semi-transparent BIPV skylight with 17 % transparency and a non-PV standard glazing have also been simulated and used as a benchmark. As expected, the conventional BIPV skylight generate a high-glare illumination inside the room (Fig. 5a), which causes a high visual discomfort. Fig. 5b) shows illumination under the smart BICPV/D module, for which the bright fringes disappear and glare is avoided. In Fig. 5c) the module is switched to high-transmission mode (solar cells moved to allow direct light transmission through the transparent backplane): the amount of daylighting is similar to a conventional window (Fig. 5d)), but much more homogeneous (*i.e.* higher visual comfort). The classical figure of merit used in concentrators to assess light uniformity is the peak-to-average ratio, which is highly related to possible glare to users [21]. A high value means low uniformity, which tend to produce visual discomfort. Table 1 summarizes the results obtained using ray tracing simulations in photometric units for the illuminance distribution on the left wall (north orientation), which is representative of the worst case where the user is facing the brightest wall. The smart BICPV/D module outperforms both the conventional BIPV skylight and the standard glazing in terms of light uniformity. In low-transmission mode, the improvement is significant, reducing the peak-to-average ratio by a factor of 6 with respect to the semi-transparent BIPV skylight, while keeping an average illuminance level suitable for easy office work (>200 lx). In high-transmission mode,

Table 1
Comparison of illuminance distributions on the North room wall.

Roofing component and configuration	Max. illuminance (lx)	Min. illuminance (lx)	Average illuminance (lx)	Peak-to-average ratio
Classical semi-transparent BIPV skylight (17 % transp.)	33836	51	1947	17
Smart BICPV/D skylight in low-transmission mode	817	19	284	2.9
Smart BICPV/D skylight in high-transmission mode	39966	165	6993	5.7
Standard glazing (no PV)	62238	234	8077	7.7

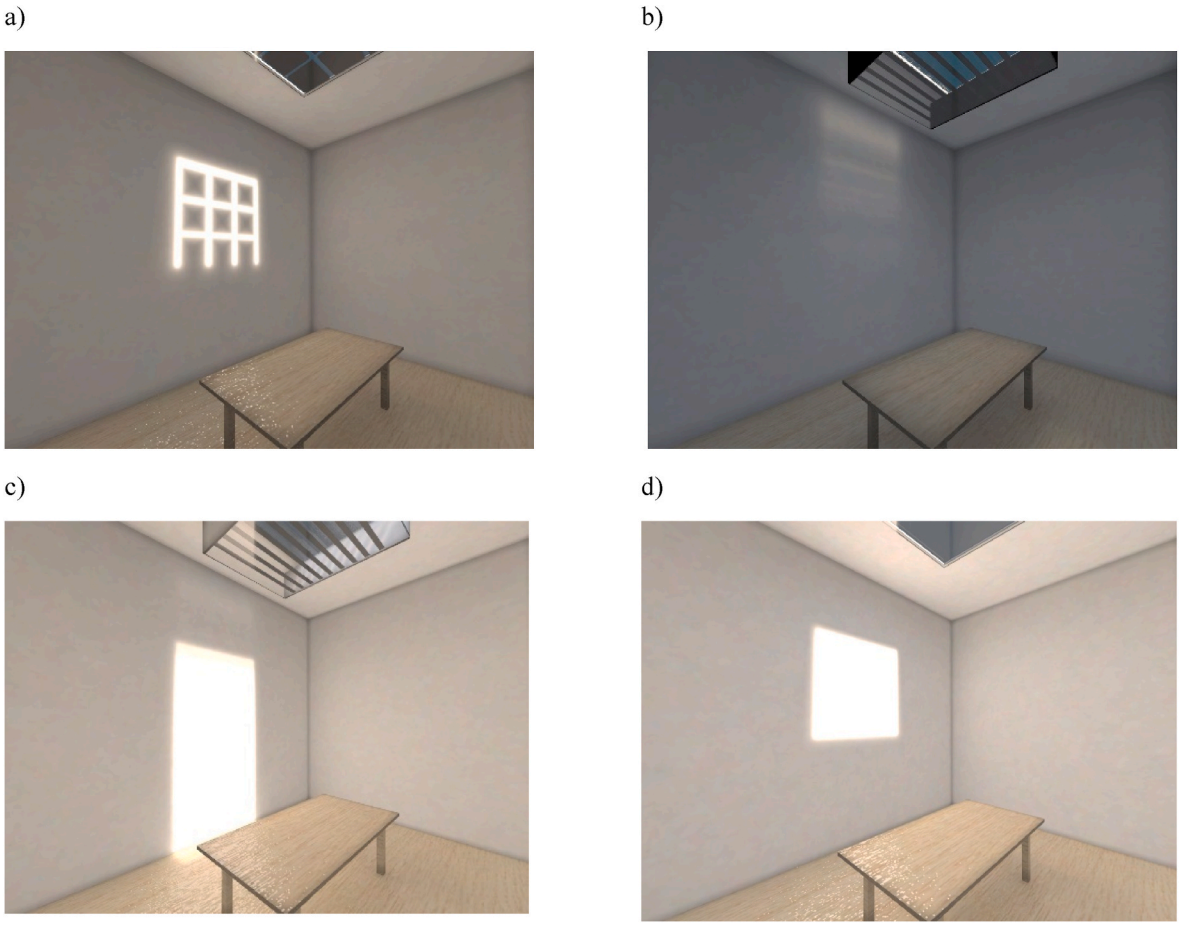

Fig. 5. Photorealistic render of **a)** a classical semi-transparent PV glazing skylight and **b)** our smart CPV module set up to produce electricity from direct light and soft homogeneous daylighting from diffuse light. **c)** When our module is set to high-transmission mode, it can increase daylighting while reducing glare or visual discomfort compared to **d)** a standard glazing skylight.

non-uniformity is reduced by 26 % compared to a standard glazing of the same size, while the average illuminance is reduced by 13 % only.

However, although glare or visual discomfort is caused by an uneven light distribution, it is actually dependent on the position and the field of view of the observer. The measurement of glare is highly subjective, as it depends on individual human perception and the unique characteristics of the environment. The unified glare rating (UGR) or the CIE glare index (CGI) are widely used indices in the illumination industry for assessing the subjective magnitude of glare discomfort. However, they were initially derived from experiments with artificial light sources exclusively, so they are not suited for scenarios with real daylighting [21]. In our study, we use daylight glare probability (DGP) instead, an index that specifically quantifies the probability that building occupants will experience discomfort glare from windows, offering a more accurate assessment for naturally lit environments [21]. For this study, we selected a scenario representing the highest potential for glare, as illustrated in Fig. 6. In this configuration, the observer is assumed to be seated at a table facing the north wall, where direct transmission of sunlight through the skylight will create the main bright spots. The wall is supposed to act as a Lambertian reflector with 80 % reflectance. The glare conditions were analyzed using the following equation:

$$DGP = c_1 Ev + c_2 \log\left(1 + \sum_i \frac{L_{s,i}^2 * \omega_{s,i}}{Ev^{c_4} * P_i^2}\right) + c_3$$

where E_V is the vertical eye illuminance [lx], which corresponds to the amount of global light reaching the subject's eyes and determines their level of adaptation to brightness. $L_{s,i}$ is the luminance [cd/m^2] of the glare sources, in this case the light reflected from the wall that illuminate the room, divided in i equal parts, whose square is multiplied by the solid angle subtended by each source fraction $\omega_{s,i}$, to represent the direct light of the source that hit the subject's vision. Lastly, P_i represents the position index, a complex relationship describing the change in the discomfort experienced due to the angular displacement of the glare source from the observer's line of sight; a careful description of how to calculate P_i can be found elsewhere [21]. The rest of the parameters are a set of constants that were empirically fitted through more than 70 subjects in two separate experiments in Ref. [21]: $c_1 = 5.87 \cdot 10^{-5}$, $c_2 = 9.18 \cdot 10^{-2}$, $c_3 = 0.16$, $c_4 = 1.87$. The DGP scale range oscillates between 0.2 (imperceptible glare) and 0.8 (intolerable glare).

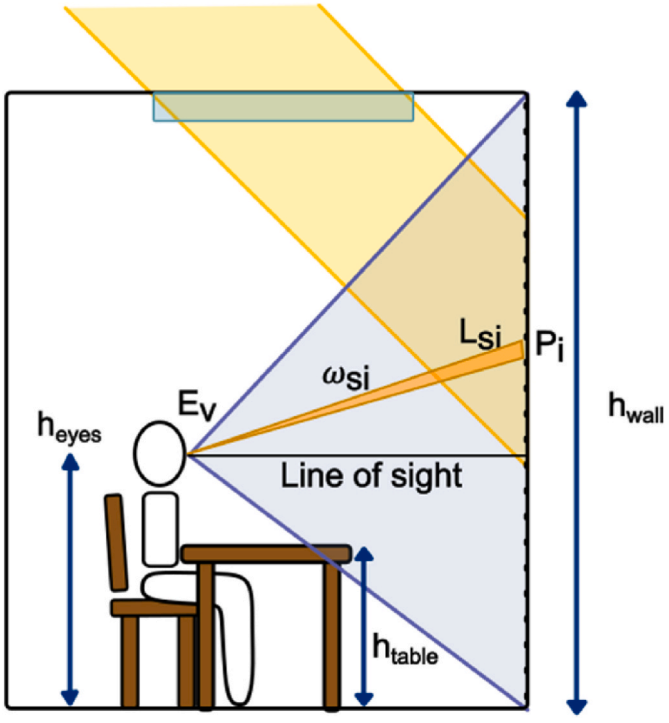

Fig. 6. Schematic representation of the simulated setup where the occupant is seated at a table facing the brightest wall (north). The dimensions of this scene are representative of a standard small room at 1:5 scale to reduce the number of lenses to simulate and save computational power. In this configuration, the wall height (h_{wall}) is 60 cm (corresponding to 3 m in full scale), the eye level height (h_{eyes}) is 25 cm (1.25 m), and the table height (h_{table}) is 15 cm (0.75 m). E_V is the vertical eye illuminance [lx], which corresponds to the amount of global light reaching the subject and controls eye adaptation levels. $L_{s,i}$ is the luminance [cd/m^2] of the glare sources, in this case the light reflected from the wall divided in i equal parts with a subtended solid angle $\omega_{s,i}$. P_i represents a position index that describes the angular displacement of the source from the observer's line of sight.

Table 2 displays the results for each configuration. In the low illumination situations, the semi-transparent BIPV skylight presents a noticeable glare (0.3) while the BICPV/D smart module shows no significant glare (0.2, a 33 % reduction). In the high illumination condition, both options generate an intolerable glare, but DPG is reduced by 15 % under the illumination of the BICPV/D module. These results demonstrate that the system is capable of producing low-glare daylighting that can be modulated following user's needs and ambient conditions. Thus, the system reduces the need for artificial lighting and improves the energy balance of the building.

5. Conclusions

The design of a novel building-integrated concentrator photovoltaics module for the simultaneous generation of solar electricity and comfortable daylighting (BICPV/D) has been presented. The module uses static linear Fresnel lenses to concentrate direct irradiance onto an array of c-Si solar cell strips (10X) on a transparent backplane. The focal lines will shift with the solar position throughout the day, so a planar micro-tracking system moves the backplane to capture concentrated light. In contrast, the diffuse irradiance is transmitted through the backplane to provide homogeneous illumination within the building with low glare. Thus, the module can provide a high power density because all the direct light incident on the aperture area is collected by the solar cells, in contrast with classical semi-transparent BIPV modules where the solar cells are spaced to allow some light transmission for daylighting. The optical design has been tailored to ultraviolet roll-to-plate imprinting processes to enable low-cost, high-throughput production. Thanks to the compactness of the design, the concept can be integrated as many different components of the building envelope: horizontal skylights or canopies, vertical curtain walls and other exterior elements such as parapets or solar shading.

Its functionality has been demonstrated through comprehensive ray-tracing simulations, with very promising results: the optical efficiency is higher than 70 % across a wide range of angles of incidence, ensuring

Table 2
Comparison of the daylight glare probability (DGP) for the worst-case situation: a person sitting at a table facing the bright wall.

Type of glazing and configuration	Vertical eye illuminance Ev (lx)	Visual discomfort DGP	Change in DGP under BICPV/D	
Classical semi-transparent BIPV skylight (17 % transp.)	2226	0.30	Low illumination	−33 %
Smart BICPV/D skylight in low-transmission mode	696	0.20		
Standard glazing (no PV)	9545	0.73	High illumination	−15 %
Smart BICPV/D skylight in high-transmission mode	7652	0.62		

high electrical efficiency and power density throughout the day in all seasons. Furthermore, photometric ray-tracing and photorealistic renderings of a reference office scene with the module integrated as a skylight demonstrates improved illuminance uniformity and lower glare compared to a conventional semi-transparent glazing with c-Si solar cells, resulting in higher visual comfort for users, a reduction of the need for artificial lighting and higher electricity generation at the same time. These simultaneous gains can encourage more building designers to integrate BIPV in their projects, thus accelerating the transition to a low-carbon urban landscape.

Ongoing work is focused on developing the first prototypes of the optical system in collaboration with IMDEA Nanoscience, optimizing the electrical layout of the solar cells and designing the mechanical integration of BICPV/D concept as different building components (curtain wall and skylight).

CRediT authorship contribution statement

Almudena Garcia-Sanchez: Writing – review & editing, Writing – original draft, Visualization, Validation, Software, Methodology, Investigation, Formal analysis, Data curation. **Guido Vallerotto:** Writing – review & editing, Visualization, Validation, Supervision, Software, Methodology, Investigation, Formal analysis, Data curation. **Steve Askins:** Software, Conceptualization. **Ignacio Antón:** Visualization, Supervision, Resources, Funding acquisition, Conceptualization. **César Domínguez:** Writing – review & editing, Visualization, Validation, Supervision, Software, Resources, Project administration, Methodology, Investigation, Funding acquisition, Formal analysis, Data curation, Conceptualization.

Declaration of competing interest

The authors declare that they have no known competing financial interests or personal relationships that could have appeared to influence the work reported in this paper.

Acknowledgements

This work has been supported by project grants MICROBEAM ref. PID2021-127810OB-I00, funded by MCIN/AEI/10.13039/501100011033 “ERDF A way of making Europe” and SMARTWIN TED2021-130920B-C21, funded by MCIN/AEI/10.13039/501100011033 and by the “European Union NextGenerationEU/PRTR”.

Data availability

Data will be made available on request.

References

[1] A. Jäger-Waldau, I. Kougias, N. Taylor, C. Thiel, How Photovoltaics Can Contribute to GHG Emission Reductions of 55% in the EU by 2030, Elsevier Ltd., Jul. 01, 2020, https://doi.org/10.1016/j.rser.2020.109836.
[2] A. Passera, P. Di Milano, S. Avesani, M. Lovati, BIPV FACADES: MARKET POTENTIAL OF RETROFIT APPLICATION IN THE EUROPEAN BUILDING STOCK, 2018, https://doi.org/10.13140/RG.2.2.24051.63528.
[3] D. Valencia-Caballero, et al., Performance analysis of a novel building integrated low concentration photovoltaic skylight with seasonal solar control, J. Build. Eng. 54 (Aug. 2022), https://doi.org/10.1016/j.jobe.2022.104687.
[4] D.S. Pillai, V. Shabunko, A. Krishna, A Comprehensive Review on Building Integrated Photovoltaic Systems: Emphasis to Technological Advancements, Outdoor Testing, and Predictive Maintenance, Elsevier Ltd., Mar. 01, 2022, https://doi.org/10.1016/j.rser.2021.111946.
[5] G. Li, Q. Xuan, M.W. Akram, Y. Golizadeh Akhlaghi, H. Liu, S. Shittu, Building Integrated Solar Concentrating Systems: A Review, Elsevier Ltd., Feb. 15, 2020, https://doi.org/10.1016/j.apenergy.2019.114288.
[6] K.N. M, N. N, E.M. A, D.A. Raugei, Life cycle assessment of an ecological living module equipped with conventional rooftop or integrated concentrating photovoltaics, J. Ind. Ecol. 25 (5) (2021) 1207–1221.
[7] T.K. Mallick, P.C. Eames, Design and fabrication of low concentrating second generation PRIDE concentrator, Sol. Energy Mater. Sol. Cell. 91 (7) (Apr. 2007) 597–608, https://doi.org/10.1016/j.solmat.2006.11.016.
[8] K. Yoshioka, S. Goma, S. Hayakawa, T. Saitoh, Preparation and properties of an experimental static concentrator with a new three-dimensional lens, Prog. Photovoltaics Res. Appl. 5 (2) (1997) 139–145, https://doi.org/10.1002/(SICI)1099-159X(199703/04)5:2<139::AID-PIP161>3.0.CO;2-2.
[9] F. Muhammad-Sukki, et al., Mirror symmetrical dielectric totally internally reflecting concentrator for building integrated photovoltaic systems, Appl. Energy 113 (2014) 32–40, https://doi.org/10.1016/j.apenergy.2013.07.010.
[10] H. Baig, N. Sellami, T.K. Mallick, Performance modeling and testing of a building integrated concentrating photovoltaic (BICPV) system, Sol. Energy Mater. Sol. Cell. 134 (2015) 29–44, https://doi.org/10.1016/j.solmat.2014.11.019.
[11] E.D. Mammo, N. Sellami, T.K. Mallick, Performance analysis of a reflective 3D crossed compound parabolic concentrating photovoltaic system for building façade integration, Prog. Photovoltaics Res. Appl. 21 (5) (Aug. 2013) 1095–1103, https://doi.org/10.1002/pip.2211.
[12] Y. Wu, K. Connelly, Y. Liu, X. Gu, Y. Gao, G.Z. Chen, Smart solar concentrators for building integrated photovoltaic façades, Sol. Energy 133 (Aug. 2016) 111–118, https://doi.org/10.1016/j.solener.2016.03.046.
[13] Y. Tripanagnostopoulos, C. Siabekou, J.K. Tonui, The Fresnel lens concept for solar control of buildings, Sol. Energy 81 (5) (May 2007) 661–675, https://doi.org/10.1016/j.solener.2006.08.013.
[14] E.M. Kritchman, A.A. Friesem, G. Yekutieli, A fixed fresnel lens with tracking collector, Sol. Energy 27 (1) (1981) 13–17.
[15] D. Chemisana, M. Ibáñez, J. Barrau, Comparison of Fresnel concentrators for building integrated photovoltaics, Energy Convers. Manag. 50 (4) (Apr. 2009) 1079–1084, https://doi.org/10.1016/j.enconman.2008.12.002.
[16] N. Jost, et al., Fabrication of high-performance lens arrays for micro-concentrator photovoltaics using ultraviolet imprinting, Int. J. Adv. Manuf. Technol. 131 (12) (Apr. 2024) 5961–5970, https://doi.org/10.1007/s00170-024-13350-z.
[17] M. Victoria, New Concepts and Techniques for the Development of High-Efficiency Concentrating Photovoltaic Modules, 2014, https://doi.org/10.13140/RG.2.1.3621.2328.
[18] E. Lorenzo, J.C. Mi, Design of one-AXIS tracked linear fresnel lenses, Sol. Energy 36 (6) (1986) 531–534.
[19] E.M. Kritchman, A.A. Friesem, G. Yekutieli, Efficient fresnel lens for solar concentration, Sol. Energy 22 (2) (1978) 119–123.
[20] R. Leutz, A. Suzuki, A. Akisawa, T. Kashiwagi, Design of a nonimaging fresnel lens for solar concentrators, Sol. Energy 65 (6) (1999) 379–387 [Online]. Available: www.elsevier.com/locate/solener.
[21] J. Wienold, J. Christoffersen, Evaluation methods and development of a new glare prediction model for daylight environments with the use of CCD cameras, Energy Build. 38 (7) (Jul. 2006) 743–757, https://doi.org/10.1016/j.enbuild.2006.03.017.